Do surface temperature indices reflect trends in Atlantic Meridional Overturning Circulation strength?

Christopher M. Little[1], Mengnan Zhao[1], Martha W. Buckley[2]

[1]Atmospheric and Environmental Research, Inc., Lexington, MA, USA.

[2]George Mason University, Fairfax, VA, USA

Key Points:

- Previously proposed surface temperature indices (STIs) of AMOC strength are dominated by global temperature trends
- STIs are poor predictors of AMOC strength outside their calibration period, calling into question previous interpretations of 20th c. trends
- Over centennial timescales, AMOC/STI relationships are sensitive to the nature of external forcing and unforced variability

Corresponding author: Christopher M. Little, clittle@aer.com

Abstract

The difference between North Atlantic subpolar gyre sea surface temperatures (SPG SSTs) and hemispheric- or global-scale surface temperatures has been utilized as an index of centennial-timescale changes in Atlantic Meridional Overturning Circulation (AMOC) strength. Here, using Community Earth System Model ensembles, we show that surface temperature-based indices (STIs) proposed to date largely reflect global-scale temperature trends and thus do not reflect dynamical relationships with AMOC. More broadly, we find that relationships between STIs, SPG SSTs, and AMOC strength differ greatly in significance and magnitude over different time periods because they are dependent upon the nature of external forcing. In the 20th century, characterized by offsetting greenhouse gas and aerosol forcing, the relationship between SSTs and AMOC strength varies widely and changes sign across a 20-member ensemble. We conclude that STIs and SPG SSTs are poor predictors of centennial-timescale AMOC strength variations.

Plain Language Summary

The short observational record of the Atlantic Meridional Overturning Circulation (AMOC) limits our ability to assess changes in its strength over the instrumental and pre-instrumental periods. Indirect proxies of ocean circulation are thus required to make inferences about past trends, e.g. those over the past century. Several previous analyses have used surface temperature indices to interpret 20th century AMOC trends. However, the robustness of this indirect AMOC proxy, including its sensitivity to time period, timescale, and/or climate state, has not been assessed.

We use two state-of-the art climate model ensembles to assess AMOC/surface temperature relationships over century timescales, finding a strong dependence upon time period and climate forcing. Our results clarify the origins of discrepancies in AMOC/surface temperature relationships and suggest that interpretations of 20th century climate and ocean circulation change based on surface temperature indices are limited.

1 Introduction

Sea surface temperatures (SSTs) are influenced by many factors, including sensible and latent air-sea heat fluxes, short and long wave radiation, and ocean heat transport due to processes such as Ekman pumping, vertical mixing and horizontal advection

(e.g. Bjerknes, 1964; Frankignoul, 1985; Chen et al., 1994; Webster et al., 2005; Pardo & Prez, 2011; Buckley et al., 2014, 2015; Buckley & Marshall, 2016). These factors interact and control SST variability at different scales. Over multidecadal and longer timescales, ocean advection is an important influence on SSTs (Bjerknes, 1964; Gulev et al., 2013). For example, low-frequency, basin-wide, SST changes, commonly referred to as Atlantic Multidecadal Variability, are generally thought to be related to variability of the Atlantic Meridional Overturning Circulation (AMOC) (Delworth et al., 2007; Deser et al., 2010; Zhang et al., 2019) (although recent work has called this assumption into question (Clement et al., 2015)). This implies that SSTs may act as fingerprints of multi-decadal to millennial changes in ocean circulation and climate, for which observational records are limited (Kravtsov & Spannagle, 2008; De Boer et al., 2010; Williams et al., 2014; Rahmstorf et al., 2015; Caesar et al., 2018).

Over centennial timescales, many studies have noted a "warming hole", or "cold patch", in the North Atlantic subpolar gyre (SPG). In some model simulations, this SST pattern has been related to changes in the AMOC (Marshall et al., 2015; Winton et al., 2013; Caesar et al., 2018), although other studies indicate that AMOC-SST relationships, including the appearance of the warming hole, depend upon climate forcing (Roberts et al., 2013). In particular, the role of AMOC changes in the warming hole over the 20th century is debated: some studies assert that the warming hole is related to an AMOC decline (Dima & Lohmann, 2010; Rahmstorf et al., 2015), while others conclude that the warming hole cannot be fully attributed to relatively modest AMOC changes in the 20th century (S. Drijfhout et al., 2012; Woollings et al., 2012).

Rahmstorf et al. (2015) (R15 hereafter) argue that the difference between SPG SST and Northern Hemisphere mean surface air temperature (NHT) (a measure of the "warming hole") reflects AMOC strength changes. To test this hypothesis, R15 perform a linear regression of this surface-temperature based index (STI) against the maximum AMOC strength using MPI-ESM-MR climate model output over the 1850–2100 period. The resulting regression coefficient (2.3 Sv/K) is then used to reconstruct AMOC from instrumental and proxy surface temperature records. However, while the correlation coefficient found by R15 was high (0.90), it was largely determined by out-of-phase trends in NHT and AMOC strength over the strongly greenhouse gas (GHG)-forced 21st century period (their Fig. 2). The AMOC/STI relationship in the model over the 20th century appears significantly weaker.

Using 15 CMIP5 models, Caesar et al. (2018) (C18 hereafter) find that the AMOC/STI relationship varies widely across climate models over the 20th century: the ratio of linear trends in AMOC strength to those in a STI (defined as the difference between winter-season SPG SSTs and global mean SST) ranges from -105 to 10 Sv/K across models (0.6 to 10 Sv/K for the 12 models determined to have a realistic representation of AMOC; see their extended Table 1). Six CMIP5 models were found to simulate large changes in AMOC (decreases of more than 1.5 Sv) and STI (decreases of more than 0.4 K) over the 1870-2016 period, with the other six showing much smaller changes in both quantities.

Here, we examine centennial-timescale relationships between sea surface temperatures, surface air temperatures, and AMOC strength using output from the Community Earth System Model Large (LE) (Kay et al., 2015) and Single Forcing (SF) (Deser et al., n.d.) Ensembles. These simulations allow AMOC/STI relationships to be assessed under different external forcings, clarifying the origins of discrepancies in scaling coefficients and the limitations of STIs as predictors of AMOC changes.

2 Methods

The Community Earth System Model Large (LE) and Single Forcing (SF) Ensembles are coordinated numerical simulations of the Earth system conducted using the CESM1 climate model, in which the Community Atmosphere Model, version 5, is coupled to the Parallel Ocean Program version 2 (POP2) model at approximately 1° horizontal resolution. Additional model components, and details of the model configuration and parameterizations are more completely described in Kay et al. (2015), and references within.

The LE consists of 40 ensemble members. Ensemble member #1 is forced with time-evolving climate forcings (e.g. greenhouse gases, aerosols, ozone, land use changes) over the 1850-2100 period, following an 1801 year control run forced with constant (1850) preindustrial forcing. To generate the 40-member initial condition ensemble, perturbations of order 10^{-14} K are applied to the air temperature state of ensemble member #1 on January 1, 1920. Identical external forcing over the 1920-2100 period is the applied to all ensemble members. However, the climate of each ensemble member evolves differently due to differences in the initial state. Taking the arithmetic mean of each quantity across ensemble members allows the identification of an "externally-forced" response. In this

analysis, to keep the same number of simulations available for the "all forcings" and single forcing experiments, we use only LE members #1-20.

In the SF ensemble, the same experimental strategy is applied, except a single forcing agent (e.g. greenhouse gases) is held at the preindustrial value, allowing an attribution of the changes in climate due to each agent. Here, we examine the changes in quantities of interest associated with GHG (greenhouse gas) and AER (industrial aerosol) forcing, using the methods of Deser et al. (2020). More details regarding both CESM ensembles are available in Kay et al. (2015) and Deser et al. (2020).

We use the maximum value of the zonally integrated overturning streamfunction north of the Equator in the Atlantic basin, and below 500 m depth, as a metric of AMOC (AMOC_{MAX}). We calculate area-averaged SSTs over the SPG region (SST_{SPG}; Fig. 1, following C18) and the area-averaged northern hemisphere air temperature (NHT; 0°–90°N); the suface temperature index (STI) is defined as the difference between SST_{SPG} and NHT (following R15). Prior to calculating trends and regression coefficients, we remove drift in CESM-LE by computing a least-squares trend fit to each variable (SST_{SPG}, NHT and AMOC_{MAX}) from the control run. This trend (-1.1x10^{-1} Sv/century for AMOC_{MAX}; -1.5x10^{-2} K/century for SST_{SPG}; -1.4x10^{-3} K/century for NHT) is then removed from individual ensemble members for each variable. Regression coefficients in Table 1 and Supplementary Table 1 are calculated using a geometric mean regression.

We compare LE simulations to NHT reconstructions from two datasets: Goddard Institute for Space Studies Surface Temperature Analysis (GISTEMP) and Climate Research Unit and Hadley Center Surface Temperature (HadCRUT4). The two datasets are not fully independent; differences stem largely from their treatment of spatial and temporal gaps in the temperature record. SST_{SPG} reconstructions are computed as the spatial mean of SST over the SPG region from two datasets: Extended Reconstructed Sea Surface Temperature (ERSSTv5, generated from International Comprehensive Ocean-Atmosphere Data Set, incorporated to GISTEMP) and Hadley Center Sea Ice and Sea Surface Temperature (HadISST, incorporated into HadCRUT4). Details of these datasets are available elsewhere (Morice et al., 2012; Lenssen et al., 2019).

3 Comparison of CESM-LE output with instrumental-era reconstructions

We first compare temperature anomalies (relative to a 1920-1970 baseline period) from 20 LE members to observational surface temperature reconstructions. The annual mean R15 STI is shown in Fig. 1a; its individual components (SST_{SPG} and NHT, see Methods) are shown in Figs. 1b and 1c, respectively. In the presence of internal variability, individual LE members are not expected to reproduce observations; we thus compare consistency between the range of trends across the simulations and the range of observational estimates. Model output is shown using the ensemble median (to limit the importance of outliers) and uncertainty (the standard deviation across each 20 simulation ensemble).

Observations (orange lines) and LE simulations (blue shading, with the blue line representing ensemble member #1; the only member available over the 1850-1919 period) indicate multidecadal to centennial variability superimposed on substantial higher-frequency variability in all quantities over the 20th century. After 1920, when the LE is initiated, observed variability almost always falls within the range of LE simulations.

Both surface temperature reconstructions and the LE indicate that STI declined over the 20th century. Before ∼2000, multidecadal variability is evident in all quantities, in observations and the LE. Subtracting NHT from SST_{SPG} removes some of the shared multidecadal variability in each quantity, leaving the trend most prominent. In the LE, AMOC strength ($AMOC_{MAX}$; see Methods) exhibits multidecadal variability on the order of a few Sv; longer-term trends, while negative, are not significant (-0.94±1.5 Sv/century over the 1921-2000 period; Fig. 1d). In the 21st century in LE (note different axes after 2000), both SST_{SPG} and NHT exhibit large increasing trends (1.1±0.25 and 5.4±0.11 K/century, respectively), opposite in sign to $AMOC_{MAX}$, which decreases by 12.3±0.98 Sv/century.

Over the 1920-2018 period, linear trends in all temperature indices show good agreement between observations and the LE. The LE STI trend is -0.87±0.14 K/century, consistent with observational reconstructions (-0.87 to -1.2 K/century). For SST_{SPG}, the LE trend is -0.11±0.14 K/century, again consistent with observational estimates (-0.11 and 0.02 K/century). In both the reconstructions and the LE, the mean SST_{SPG} trend is small compared to those in STI, and less than its standard deviation across the 20-

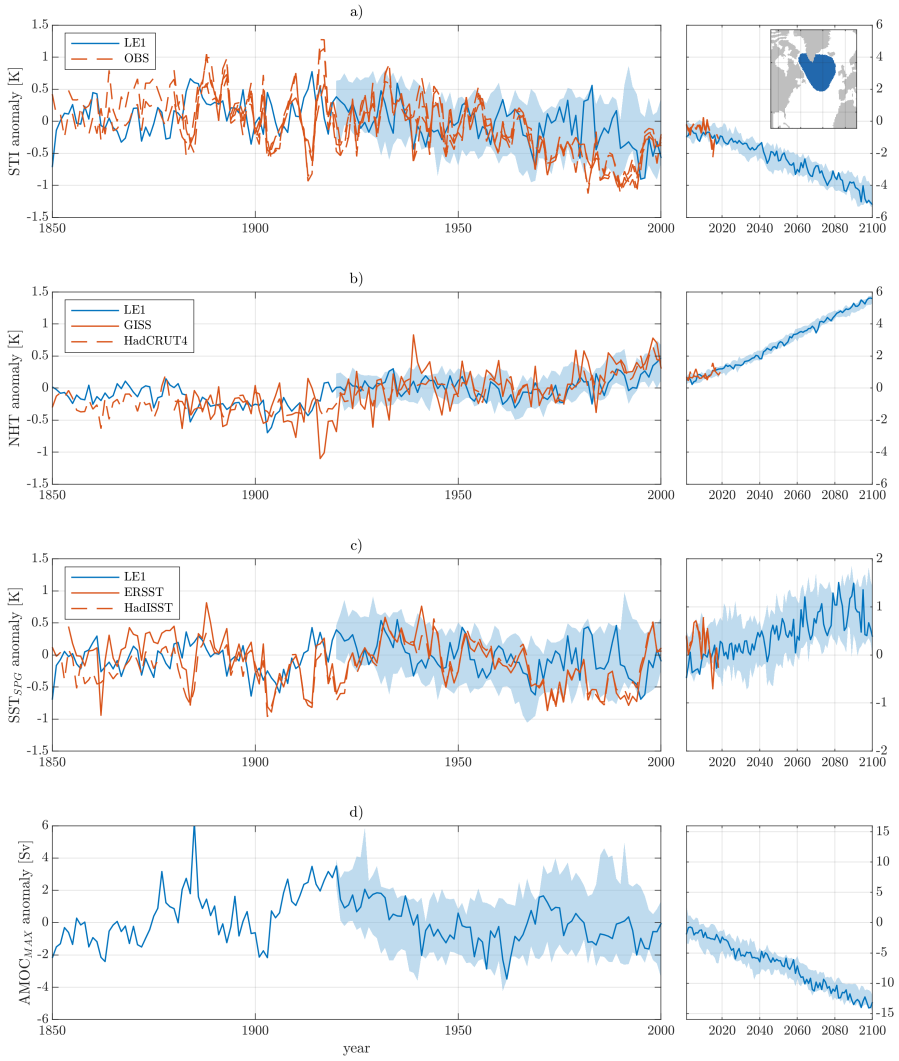

Figure 1. Annual mean a) STI, b) NHT, and c) SST$_{SPG}$ from LE simulations (blue shading is the ensemble range and blue line is ensemble member #1), and various observational reconstructions (orange lines, described in Methods). Since there are two observational products used for NHT and SST$_{SPG}$, there are 4 STI estimates. Inset in (a) shows the region over which SST$_{SPG}$ is calculated (blue shading). d) Annual mean AMOC$_{MAX}$ (in Sv) from LE simulation #1. All values are anomalies from a 1920-1970 baseline. Note axes scales are different before and after 2000.

member ensemble, whereas NHT trends are almost always positive and similar in magnitude to STI trends. This comparison thus indicates that: 1) CESM-LE trends in surface temperature indices are consistent with the range of observed trends over the 1920-2018 period, and 2) STI is predominantly controlled by increases in NHT, rather than SST changes in the warming hole region. The latter result weakens the argument that the STI is dynamically related to AMOC changes.

4 Forcing-dependence of AMOC/STI relationships

We examine the AMOC/STI relationship for each LE member using a linear regression-based approach over the 1921-2080, 1921-2000, and 2001-2080 periods (see Table 1 and Methods). For direct comparison with R15, we perform the same analysis for ensemble member #1 over the 1850-2100 period. Linear regression over the 1921-2080 period shows a strong AMOC/STI relationship (r^2_{STI}=0.91±0.01) with a coefficient (α_{STI}) of 3.0±0.01 Sv/K (slightly higher than the value found by R15 using the MPI-MR model, with a similar correlation coefficient). However, regression coefficients differ substantially between 1921-2000 (ensemble mean 4.0 Sv/K) and 2001-2080 (ensemble mean 2.8 Sv/K). There is a sharp contrast in the significance of the regression coefficient between the 1921-2000 and 2001-2080 periods, with the earlier period indicating a very weak relationship (r^2=0.05±0.09).

The AMOC/STI relationship over the entire period is thus largely controlled by the trends over the 21st century. Furthermore, when the relationship is strong (i.e. the 21st century), the AMOC/STI relationship is controlled by the NHT; in fact, the inclusion of SST_{SPG} degrades the fit relative to NHT alone (r^2_{STI}=0.89±0.02; r^2_{NHT}=0.94±0.02).

Externally-forced regression coefficients differ between the 20th and 21st centuries (α_{STI}=3.6 and α_{STI}=2.8, respectively). To more clearly identify the origin of this difference, we utilize the SF ensemble, in which we can separately examine AMOC/STI relationships associated with each of the dominant 20th century forcings: greenhouse gases (GHG) and industrial aerosols (AER). Time series of STI, NHT, SST_{SPG}, and AMOC_{MAX} are shown for 20 LE, GHG, and AER simulations in Fig. 2 (shading indicates the $\pm 1\sigma$ range across each ensemble, lines indicate the ensemble mean, which approximates the externally-forced response). Although unforced decadal to multidecadal variability is present in all simulations, particularly in SST_{SPG} and AMOC_{MAX}, externally-forced variations are most evident at the longest (centennial) timescales. Externally-forced trends in SST_{SPG}

Table 1. Trends in AMOC_{MAX} and STI for each LE simulation, and coefficients (α) and goodness-of-fit (r^2) for regressions of AMOC_{MAX} against STI and NHT. Each column shows the median $\pm 1\sigma$ range across the LE simulations. Externally-forced (ensemble mean) values for the LE and SF simulations are shown in the lower panel.

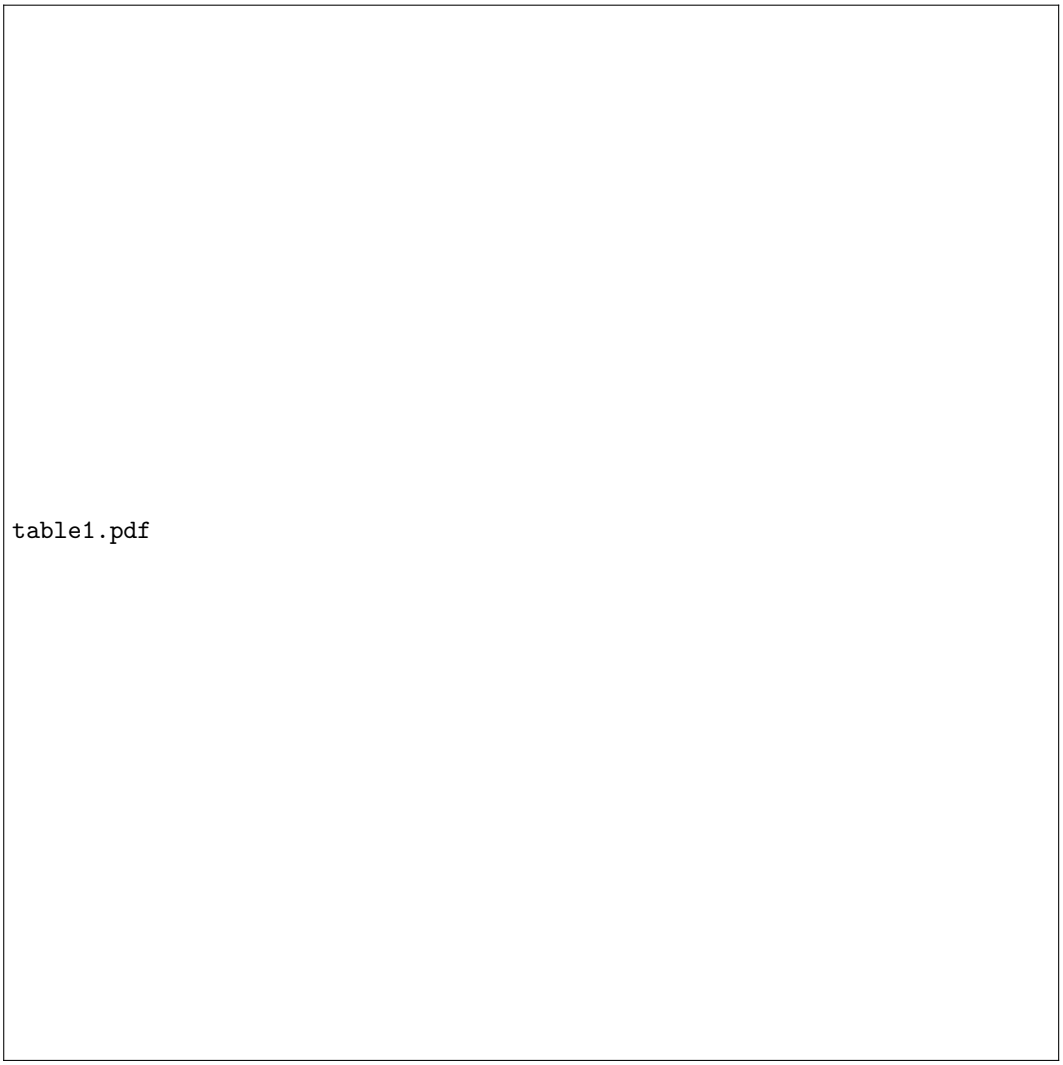

198 are generally negligible relative to internal variability, with the exception of a GHG-forced
199 increase in the second half of the 21st century. Trends in STI are, as in the "all-forcings"
200 simulations, consistently dominated by trends in NHT.

201 As expected, greenhouse gas forcing leads to increases in NHT and declines in AMOC_{MAX}
202 through the entire simulation (S. S. Drijfhout & Hazeleger, 2007; S. Drijfhout et al., 2008).
203 The temporal evolution of surface temperature and AMOC strength is more complex un-
204 der aerosol forcing: in the 20th century, increasing aerosol concentrations drive decreases
205 in NHT and increases in AMOC_{MAX} (Delworth & Dixon, 2006; Menary et al., 2013),
206 especially over the 1950-2000 period. In the 21st century, reductions in aerosol concen-
207 trations after ∼2000 are associated with trends in the AMOC and STI of similar mag-
208 nitude but of opposite sign. Thus, AER- and GHG- induced changes are counteracting
209 in the 20th century and reinforcing in the 21st century; the magnitude of AER-induced
210 AMOC changes is comparable to GHG-induced changes in both periods.

211 Regression of the GHG-forced STI on AMOC_{MAX} (Table 1) reveals that coefficients
212 are different in the 20th (α_{STI}=2.8 Sv/K) and 21st (α_{STI}=1.9 Sv/K) centuries; signif-
213 icance levels are slightly higher for the 21st century compared to the 20th century (r^2_{STI}=0.86
214 and r^2_{STI}=0.74, respectively). Regression coefficients for AER forcing are of compara-
215 ble magnitude (α_{STI}=3.7-3.8 Sv/K) and significance (r^2_{STI}=0.82-0.86) in the 20th and
216 21st centuries. The regression coefficients are larger for AER than for GHG, reflecting
217 a larger AMOC change per unit NHT change under AER forcing.

218 Differences between externally-forced 20th and 21st century AMOC/STI relation-
219 ships thus originate from: 1) unique relationships between AMOC and surface temper-
220 ature under AER and GHG forcing; 2) nonstationary relationships under GHG forcing;
221 and 3) the time-varying relative importance of each forcing. When AER and GHG forc-
222 ing drive offsetting NHT and AMOC trends (the 20th century), surface temperature and
223 AMOC changes are very small. This leads to an overall regression coefficient that is very
224 sensitive to unforced SST and/or AMOC variability (see next section). The 21st cen-
225 tury relationship is less sensitive to internal variability, given larger externally-forced trends
226 and the reinforcing nature of AER and GHG forcing. However, the AMOC/STI rela-
227 tionship should be expected to vary in time, due both to the evolution of each forcing
228 agent and the non-stationary AMOC/STI relationship under GHG forcing.

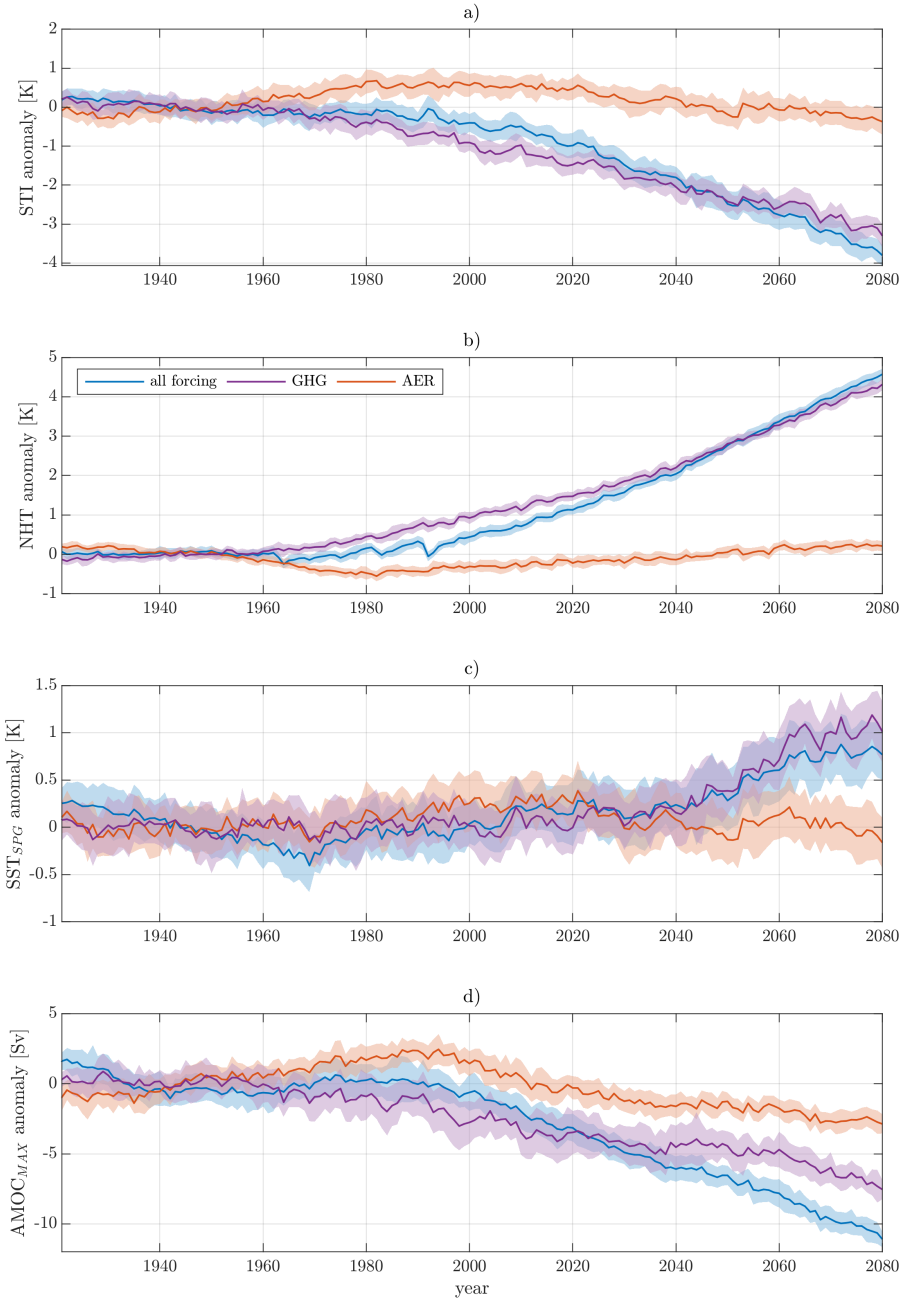

Figure 2. a) STI, b) SST$_{SPG}$, c) NHT and d) AMOC$_{MAX}$ over the 1920-2080 period for different LE and SF experiments. Ensemble mean is shown with thick lines; shading represents median $\pm 1\sigma$ range.

5 Is the "warming hole" an indicator of AMOC changes?

The previous sections show that centennial-timescale changes in STIs are controlled by large-scale (hemispheric or global), externally-forced, temperature trends. Although this result indicates that previously proposed STIs do not capture a dynamical relationship between the AMOC and SPG SSTs, it does not conflict with the prevalent idea that a "warming hole" is related to AMOC weakening (see introduction).

In the LE, a warming hole is present in both 20th and 21st century simulations, associated with an externally forced decline in AMOC_{MAX} (Figs. 3a and 3d). More generally, the presence of a SST change in the SPG opposite in sign to the radiative forcing is a consistent feature of externally-forced climate changes: for example, increases in AER forcing and AMOC_{MAX} during the 20th century are associated with warming in the SPG interior. Yet despite the consistent appearance of a warming hole under external forcing, SPG SSTs are a poor indicator of the magnitude of AMOC strength changes: SST changes due to the radiative effects of external forcing and AMOC strength counteract each other, and the degree to which they offset is forcing-dependent.

The externally-forced spatial pattern of SST trends also varies with forcing and time period. For example, the 20th century GHG-forced SST pattern (Fig. 3b) bears resemblance to that under 20th century AER forcing, but the GHG-forced "warming hole" shifts eastward in the 21st century (Fig. 3e), suggestive of an shift of the North Atlantic Current (Zhang et al., 2019). 21st century GHG forcing also results in cooling in the Northern Recirculation Gyre/Gulf Stream Extension region (Saba et al., 2016; Caesar et al., 2018), opposite in sign to the enhanced local warming evident in GHG-forced simulations in the 20th century.

When externally-forced trends are small (as in the 20th century, when AER and GHG forcings offset), the $\mathrm{SST}/\mathrm{AMOC}_{MAX}$ relationship is highly sensitive to differences resulting from internal variability. SST and AMOC_{MAX} trends vary widely across individual members of the LE over the 1921-2000 period (Fig. 4 and Supplementary Table 2), and are often opposite in sign to the externally-forced change: individual simulations show positive AMOC trends (e.g. LE #3), insignificant and/or positive SST_{SPG} trends (e.g. LE #15), and a negative trend ratio (e.g. LE #4; AMOC trends out-of-phase with SST_{SPG}). There is no obvious relationship between SSTs and AMOC_{MAX} trends

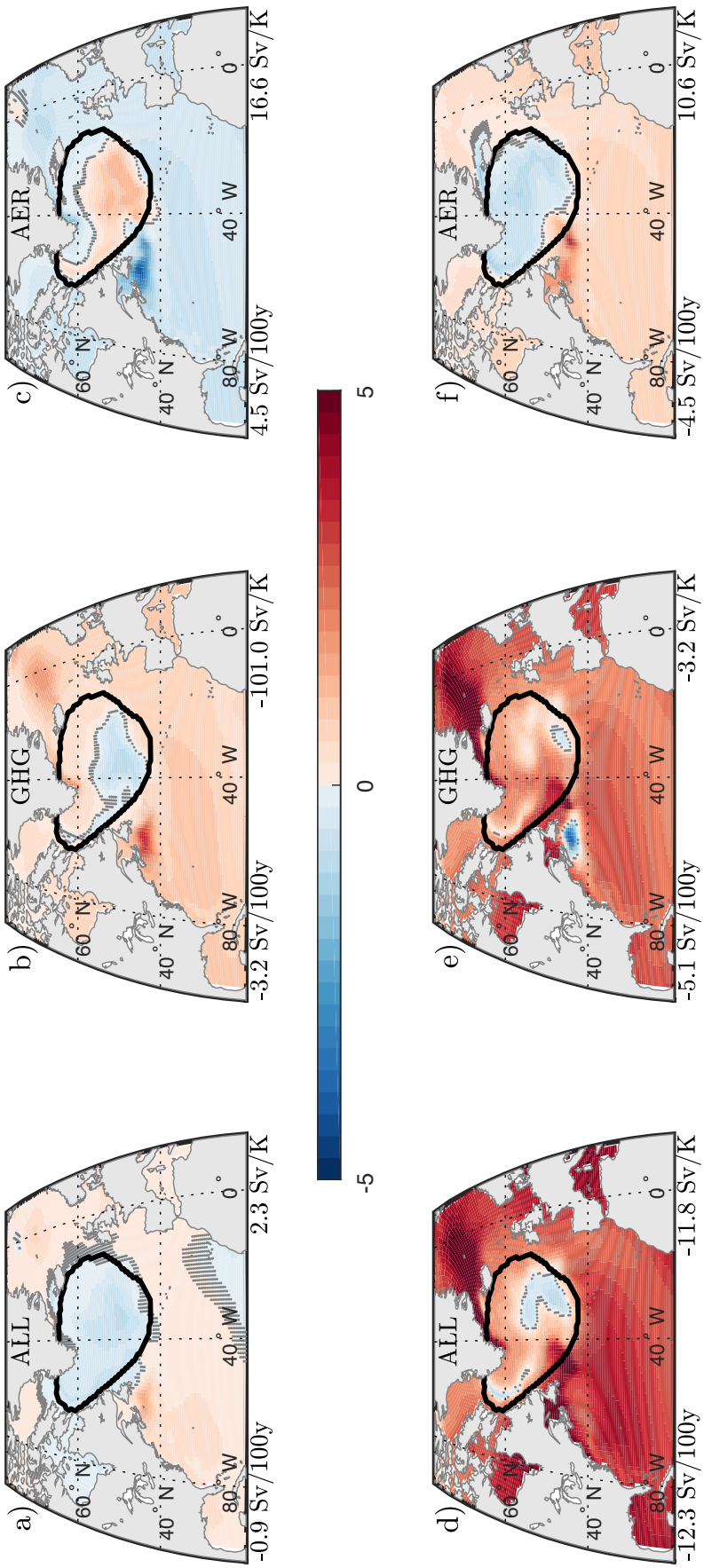

Figure 3. a-c) Ensemble mean local SST trends (K/100y) over the 1921-2000 period: a) LE; b) GHG; c) AER. d-f) as (a-c), for the 2001-2080 period. Values shown below each panel indicate (left) the ensemble mean linear trend in AMOC_{MAX} and (right) the ratio of the ensemble mean linear trend in AMOC_{MAX} to the ensemble mean linear trend in SST_{SPG}. Stippling indicates that the local SST trend is not significant at a 95% confidence level using a Mann-Kendall test.

across the ensemble. Over the SPG as a whole, the ensemble standard deviation in the $\mathrm{AMOC}_{MAX}/\mathrm{SST}_{SPG}$ trend ratio (6.1 Sv/K) is much larger than the LE mean (2.3 Sv/K).

Figs. 3 and 4 indicate that the observed trend in North Atlantic SSTs is likely to represent a convolution of AER and GHG-forced responses, and that internal variability may play a strong role in observed pattern of SST trends and their relationship with AMOC, even over centennial timescales. They also suggest that the inter-model spread in AMOC/STI relationships (as noted in the introduction) is likely to originate in the relative importance of aerosol and GHG-forced responses, as well as differences in initial states.

6 Discussion and Conclusions

Here, using Community Earth System Model ensembles, we have shown that the spatial pattern and magnitude of surface temperature trends associated with changes in AMOC strength, and thus the relationship between AMOC strength and surface-temperature indices, are dependent upon the nature of external forcing. In the 20th century, externally-forced trends in AMOC and SPG SSTs are of a comparable magnitude as those associated with natural climate system variability. Our results suggest that previously proposed STIs are not dynamically related to AMOC strength over centennial timescales; rather, their correlation predominantly reflects opposing trends in AMOC and hemispheric or global surface temperature in response to common external forcing. In formulations proposed to date, STIs are thus poor predictors of AMOC trends outside of their calibration period, calling into question previous interpretations of 20th century AMOC variability (Rahmstorf et al., 2015; Caesar et al., 2018).

It is possible that SSTs in a more geographically limited region may be more closely related to oceanic processes, including AMOC. Indeed, the southern SPG consistently shows the largest (out-of-phase with AMOC strength) SST change in Fig. 3. However, the absolute change in SSTs is insufficient as an AMOC metric: for example, there is a small warming in these regions under 21st century GHG forcing (Fig. 3e), even under a dramatic AMOC decline.

Our conclusions do not preclude the utility of suface-temperature-based indices to capture AMOC variability on multidecadal timescales (Medhaug & Furevik, 2011; Roberts et al., 2013; Muir & Fedorov, 2015; Kim et al., 2018); such an assessment deserves fur-

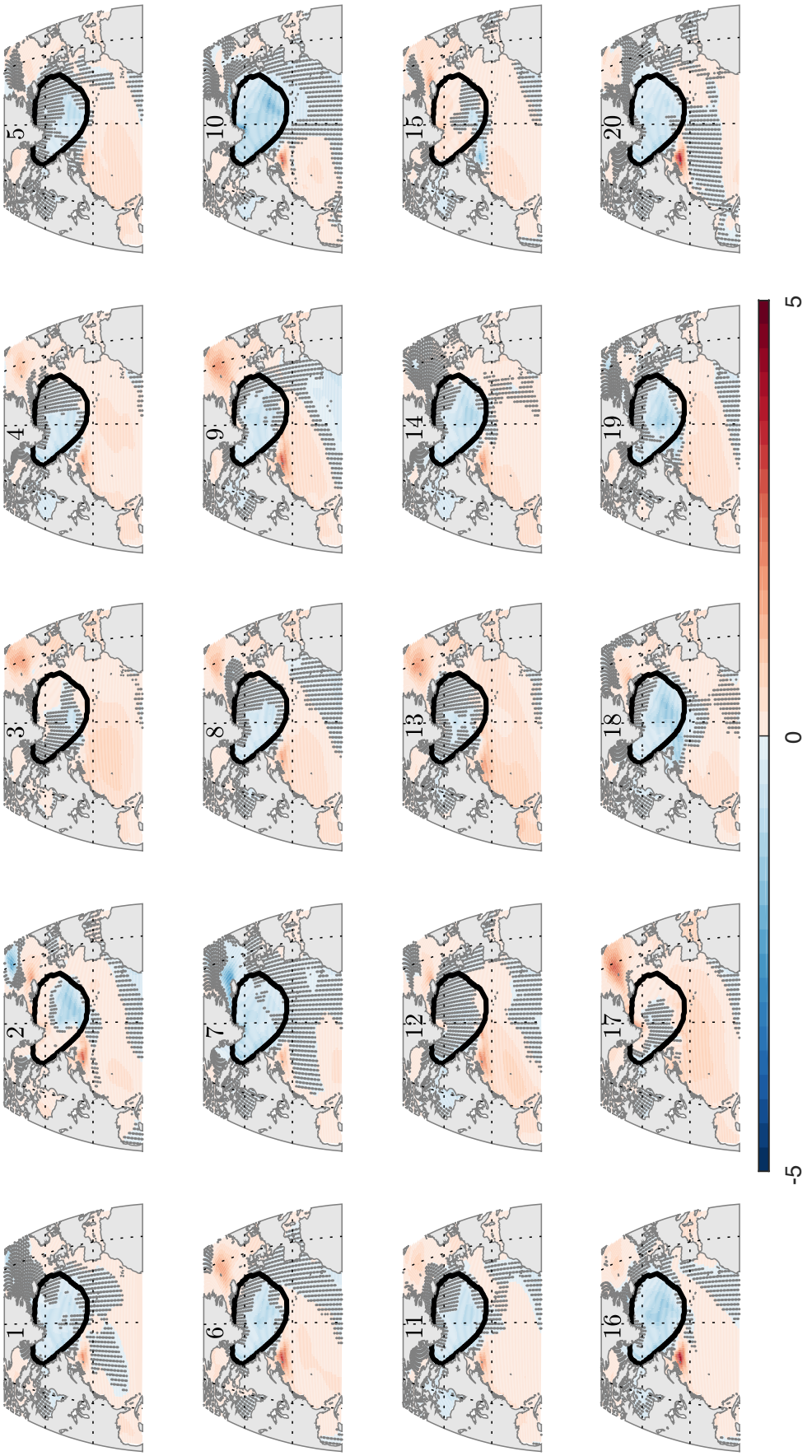

Figure 4. As Fig. 3, but for each of the 20 LE members. For each ensemble member, linear trends in AMOC_{MAX}, and the ratio of the linear trend in AMOC_{MAX} to the linear trend in SST_{SPG}, are shown in Supplementary Table 2.

ther investigation. With respect to efforts to reconstruct climate and AMOC over longer timescales, other proxies may serve as indicators of AMOC, such as subsurface densities (Roberts et al., 2013), silt records (Thornalley et al., 2018), Florida Current strength (Lund et al., 2006; Gu et al., 2020) or instrumental and proxy-derived coastal sea level records (Kopp, 2013; Kemp et al., 2017; Piecuch, 2020).

Our results reveal aspects of AMOC and SST (co-)variability deserving of further, more mechanistically-oriented, model analyses, including forcing- and time-dependent North Atlantic AMOC/SST relationships, and a high sensitivity of AMOC to 20th and 21st century aerosol forcing. The sensitivity of AMOC to aerosol forcing is likely to be related to aerosolcloud interactions, which are parameterized and potentially overestimated in current-generation climate models (e.g. Menary et al., 2020, and references within). More broadly, our results are conditional on the adequate representation of relevant physics in a coarse-resolution climate model, including: 1) cloud physics, beyond their role in aerosol indirect effects; and 2) ocean mesoscale processes, which are likely to influence AMOC and SST patterns. For some applications (including changes in Gulf Stream position and AMOC strength), models with increased horizontal resolution have been shown to exhibit qualitatively different responses to forcing (e.g. Saba et al., 2016; Hirschi et al., 2020). These caveats imply that the relationship and robustness of the forced response should be investigated with other, ideally high-resolution, climate models. However, such computationally expensive models may not have the capability to fully investigate the role of natural variability highlighted in this study.

Acknowledgments

CML and MZ acknowledge funding support from NSF Grant OCE1805029. MWB acknowledges funding support from the NOAA ESS program (NA16OAR4310167) and the NASA physical oceanography program (NNX17AH49G). The authors thank LuAnne Thompson and an anonymous reviewer for their insightful suggestions, and appreciate the extensive effort of National Center for Atmospheric Research (NCAR), the CESM Project, and CISL supercomputing resources (doi:10.5065/D6RX99HX) to produce and make available CESM-LE and SF output. All CESM output used in this paper is available via NCAR.

References

Bjerknes, J. (1964). Atlantic air-sea interaction. In *Advances in geophysics* (Vol. 10,

pp. 1–82). Elsevier.

Buckley, M. W., & Marshall, J. (2016, mar). *Observations, inferences, and mechanisms of the Atlantic Meridional Overturning Circulation: A review* (Vol. 54) (No. 1). Blackwell Publishing Ltd. doi: 10.1002/2015RG000493

Buckley, M. W., Ponte, R. M., Forget, G., & Heimbach, P. (2014, July). Low-Frequency SST and Upper-Ocean Heat Content Variability in the North Atlantic. *Journal of Climate*, *27*(13), 4996–5018. Retrieved 2018-06-26, from `http://journals.ametsoc.org/doi/abs/10.1175/JCLI-D-13-00316.1` doi: 10.1175/JCLI-D-13-00316.1

Buckley, M. W., Ponte, R. M., Forget, G., & Heimbach, P. (2015, May). Determining the Origins of Advective Heat Transport Convergence Variability in the North Atlantic. *Journal of Climate*, *28*(10), 3943–3956. Retrieved 2018-06-26, from `http://journals.ametsoc.org/doi/10.1175/JCLI-D-14-00579.1` doi: 10.1175/JCLI-D-14-00579.1

Caesar, L., Rahmstorf, S., Robinson, A., Feulner, G., & Saba, V. (2018). Observed fingerprint of a weakening Atlantic Ocean overturning circulation. *Nature*, *556*(7700), 191–196. doi: 10.1038/s41586-018-0006-5

Chen, D., Busalacchi, A. J., & Rothstein, L. M. (1994). The roles of vertical mixing, solar radiation, and wind stress in a model simulation of the sea surface temperature seasonal cycle in the tropical Pacific Ocean. *Journal of Geophysical Research: Oceans*, *99*(C10), 20345–20359. doi: https://doi.org/10.1029/94JC01621

Clement, A., Bellomo, K., Murphy, L. N., Cane, M. A., Mauritsen, T., Rdel, G., & Stevens, B. (2015). The Atlantic Multidecadal Oscillation without a role for ocean circulation. *Science*, *350*(6258), 320–324. (Publisher: American Association for the Advancement of Science)

De Boer, A. M., Gnanadesikan, A., Edwards, N. R., & Watson, A. J. (2010). Meridional density gradients do not control the atlantic overturning circulation. *Journal of Physical Oceanography*, *40*(2), 368–380.

Delworth, T. L., & Dixon, K. W. (2006). Have anthropogenic aerosols delayed a greenhouse gas-induced weakening of the North Atlantic thermohaline circulation? *Geophysical Research Letters*, *33*(2), L02606. Retrieved 2020-05-05, from `http://doi.wiley.com/10.1029/2005GL024980` doi:

10.1029/2005GL024980

Delworth, T. L., Zhang, R., & Mann, M. E. (2007). Decadal to centennial variability of the atlantic from observations and models. *Geophysical Monograph-American Geophysical Union*, *173*, 131.

Deser, C., Alexander, M. A., Xie, S.-P., & Phillips, A. S. (2010). Sea surface temperature variability: Patterns and mechanisms. *Annual review of marine science*, *2*, 115–143.

Deser, C., Phillips, A. S., Simpson, I. R., Rosenbloom, N., Coleman, D., Lehner, F., ... Stevenson, S. (n.d.). Isolating the Evolving Contributions of Anthropogenic Aerosols and Greenhouse Gases: A New CESM1 Large Ensemble Community Resource. *J. Climate*, *in review*. Retrieved from `http://www.cgd.ucar.edu/staff/cdeser/docs/submitted.deser.single\_forcing\_ensemble.feb20.pdf`

Dima, M., & Lohmann, G. (2010, January). Evidence for Two Distinct Modes of Large-Scale Ocean Circulation Changes over the Last Century. *Journal of Climate*, *23*(1), 5–16. Retrieved 2020-06-22, from `https://doi.org/10.1175/2009JCLI2867.1` doi: 10.1175/2009JCLI2867.1

Drijfhout, S., Hazeleger, W., Selten, F., & Haarsma, R. (2008, March). Future changes in internal variability of the Atlantic Meridional Overturning Circulation. *Climate Dynamics*, *30*(4), 407–419. Retrieved 2020-05-05, from `http://link.springer.com/10.1007/s00382-007-0297-y` doi: 10.1007/s00382-007-0297-y

Drijfhout, S., van Oldenborgh, G. J., & Cimatoribus, A. (2012, December). Is a Decline of AMOC Causing the Warming Hole above the North Atlantic in Observed and Modeled Warming Patterns? *Journal of Climate*, *25*(24), 8373–8379. Retrieved 2020-05-18, from `http://journals.ametsoc.org/doi/10.1175/JCLI-D-12-00490.1` doi: 10.1175/JCLI-D-12-00490.1

Drijfhout, S. S., & Hazeleger, W. (2007, April). Detecting Atlantic MOC Changes in an Ensemble of Climate Change Simulations. *Journal of Climate*, *20*(8), 1571–1582. Retrieved 2020-05-05, from `http://journals.ametsoc.org/doi/10.1175/JCLI4104.1` doi: 10.1175/JCLI4104.1

Frankignoul, C. (1985). Sea surface temperature anomalies, planetary waves, and airsea feedback in the middle latitudes. *Reviews of geophysics*, *23*(4), 231–246.

doi: https://doi.org/10.1029/RG023i004p00357

Gu, S., Liu, Z., & Wu, L. (2020, March). Time Scale Dependence of the Meridional Coherence of the Atlantic Meridional Overturning Circulation. *Journal of Geophysical Research: Oceans*, *125*(3). Retrieved 2020-04-14, from `https://onlinelibrary.wiley.com/doi/abs/10.1029/2019JC015838` doi: 10.1029/2019JC015838

Gulev, S. K., Latif, M., Keenlyside, N., Park, W., & Koltermann, K. P. (2013). North atlantic ocean control on surface heat flux on multidecadal timescales. *Nature*, *499*(7459), 464.

Hirschi, J. J., Barnier, B., Bning, C., Biastoch, A., Blaker, A. T., Coward, A., ... Xu, X. (2020, April). The Atlantic Meridional Overturning Circulation in HighResolution Models. *Journal of Geophysical Research: Oceans*, *125*(4). Retrieved 2020-09-11, from `https://onlinelibrary.wiley.com/doi/abs/10.1029/2019JC015522` doi: 10.1029/2019JC015522

Kay, J. E., Deser, C., Phillips, A., Mai, A., Hannay, C., Strand, G., ... Vertenstein, M. (2015, August). The Community Earth System Model (CESM) Large Ensemble Project: A Community Resource for Studying Climate Change in the Presence of Internal Climate Variability. *Bulletin of the American Meteorological Society*, *96*(8), 1333–1349. Retrieved 2019-03-08, from `http://journals.ametsoc.org/doi/10.1175/BAMS-D-13-00255.1` doi: 10.1175/BAMS-D-13-00255.1

Kemp, A. C., Kegel, J. J., Culver, S. J., Barber, D. C., Mallinson, D. J., Leorri, E., ... others (2017). Extended late holocene relative sea-level histories for north carolina, usa. *Quaternary Science Reviews*, *160*, 13–30.

Kim, W. M., Yeager, S., Chang, P., & Danabasoglu, G. (2018). Low-frequency North Atlantic climate variability in the community earth system model large ensemble. *Journal of Climate*, *31*(2), 787–813. doi: 10.1175/JCLI-D-17-0193.1

Kopp, R. E. (2013). Does the mid-atlantic united states sea level acceleration hot spot reflect ocean dynamic variability? *Geophysical Research Letters*, *40*(15), 3981–3985.

Kravtsov, S., & Spannagle, C. (2008). Multidecadal climate variability in observed and modeled surface temperatures. *Journal of Climate*, *21*(5), 1104–1121.

Lenssen, N. J., Schmidt, G. A., Hansen, J. E., Menne, M. J., Persin, A., Ruedy, R.,

& Zyss, D. (2019). Improvements in the GISTEMP uncertainty model. *Journal of Geophysical Research: Atmospheres*, *124*(12), 6307–6326. (Publisher: Wiley Online Library)

Lund, D. C., Lynch-Stieglitz, J., & Curry, W. B. (2006, November). Gulf Stream density structure and transport during the past millennium. *Nature*, *444*(7119), 601–604. Retrieved 2018-06-27, from `http://www.nature.com/articles/nature05277` doi: 10.1038/nature05277

Marshall, J., Scott, J. R., Armour, K. C., Campin, J.-M., Kelley, M., & Romanou, A. (2015, April). The oceans role in the transient response of climate to abrupt greenhouse gas forcing. *Climate Dynamics*, *44*(7-8), 2287–2299. Retrieved 2020-05-18, from `http://link.springer.com/10.1007/s00382-014-2308-0` doi: 10.1007/s00382-014-2308-0

Medhaug, I., & Furevik, T. (2011). North Atlantic 20th century multidecadal variability in coupled climate models: Sea surface temperature and ocean overturning circulation. *Ocean Science*, *7*(3), 389–404. doi: 10.5194/os-7-389-2011

Menary, M. B., Roberts, C. D., Palmer, M. D., Halloran, P. R., Jackson, L., Wood, R. A., ... Lee, S.-K. (2013, April). Mechanisms of aerosol-forced AMOC variability in a state of the art climate model: HISTORICALLY STRENGTHENING AMOC. *Journal of Geophysical Research: Oceans*, *118*(4), 2087–2096. Retrieved 2018-06-27, from `http://doi.wiley.com/10.1002/jgrc.20178` doi: 10.1002/jgrc.20178

Menary, M. B., Robson, J., Allan, R. P., Booth, B. B. B., Cassou, C., Gastineau, G., ... Zhang, R. (2020, July). AerosolForced AMOC Changes in CMIP6 Historical Simulations. *Geophysical Research Letters*, *47*(14). Retrieved 2020-09-11, from `https://onlinelibrary.wiley.com/doi/abs/10.1029/2020GL088166` doi: 10.1029/2020GL088166

Morice, C. P., Kennedy, J. J., Rayner, N. A., & Jones, P. D. (2012, April). Quantifying uncertainties in global and regional temperature change using an ensemble of observational estimates: The HadCRUT4 data set: THE HADCRUT4 DATASET. *Journal of Geophysical Research: Atmospheres*, *117*(D8), n/a–n/a. Retrieved 2018-06-27, from `http://doi.wiley.com/10.1029/2011JD017187` doi: 10.1029/2011JD017187

Muir, L. C., & Fedorov, A. V. (2015, dec). How the AMOC affects ocean tem-

peratures on decadal to centennial timescales: the North Atlantic versus an interhemispheric seesaw. *Climate Dynamics*, *45*(1-2), 151–160. doi: 10.1007/s00382-014-2443-7

Pardo, X. A. P. M. G. L. F.-B., Paula C., & Prez, F. F. (2011). Evolution of upwelling systems coupled to the long-term variability in sea surface temperature and Ekman transport. *Climate Research*, *48*(2-3), 231–246. doi: https://doi.org/10.3354/cr00989

Piecuch, C. (2020). Weakening of the gulf stream at florida straits over the past century inferred from coastal sea-level data. *Earth and Space Science Open Archive*, 84. Retrieved from `https://doi.org/10.1002/essoar.10502506.1` doi: 10.1002/essoar.10502506.1

Rahmstorf, S., Box, J. E., Feulner, G., Mann, M. E., Robinson, A., Rutherford, S., & Schaffernicht, E. J. (2015). Exceptional twentieth-century slowdown in atlantic ocean overturning circulation. *Nature climate change*, *5*(5), 475–480.

Roberts, C. D., Garry, F. K., & Jackson, L. C. (2013). A multimodel study of sea surface temperature and subsurface density fingerprints of the Atlantic meridional overturning circulation. *Journal of Climate*, *26*(22), 9155–9174. doi: 10.1175/JCLI-D-12-00762.1

Saba, V. S., Griffies, S. M., Anderson, W. G., Winton, M., Alexander, M. A., Delworth, T. L., ... others (2016). Enhanced warming of the n orthwest a tlantic o cean under climate change. *Journal of Geophysical Research: Oceans*, *121*(1), 118–132.

Thornalley, D. J., Oppo, D. W., Ortega, P., Robson, J. I., Brierley, C. M., Davis, R., ... Keigwin, L. D. (2018). Anomalously weak Labrador Sea convection and Atlantic overturning during the past 150 years. *Nature*, *556*(7700), 227–230. doi: 10.1038/s41586-018-0007-4

Webster, P. J., Holland, G. J., Curry, J. A., & Chang, H.-R. (2005). Changes in tropical cyclone number, duration, and intensity in a warming environment. *Science*, *309*(5742), 1844–1846. doi: 10.1126/science.1116448

Williams, R. G., Roussenov, V., Smith, D., & Lozier, M. S. (2014). Decadal evolution of ocean thermal anomalies in the north atlantic: The effects of ekman, overturning, and horizontal transport. *Journal of Climate*, *27*(2), 698–719.

Winton, M., Griffies, S. M., Samuels, B. L., Sarmiento, J. L., & Frlicher, T. L.

(2013, April). Connecting Changing Ocean Circulation with Changing Climate. *Journal of Climate*, *26*(7), 2268–2278. Retrieved 2020-05-18, from http://journals.ametsoc.org/doi/10.1175/JCLI-D-12-00296.1 doi: 10.1175/JCLI-D-12-00296.1

Woollings, T., Harvey, B., Zahn, M., & Shaffrey, L. (2012, December). On the role of the ocean in projected atmospheric stability changes in the Atlantic polar low region. *Geophysical Research Letters*, *39*(24), 2012GL054016. Retrieved 2020-05-18, from https://onlinelibrary.wiley.com/doi/abs/10.1029/2012GL054016 doi: 10.1029/2012GL054016

Zhang, R., Sutton, R., Danabasoglu, G., Kwon, Y.-O., Marsh, R., Yeager, S., ... Little, C. (2019). A review of the role of the atlantic meridional overturning circulation in atlantic multidecadal variability and associated climate impacts. *Reviews of Geophysics*, *57*(2), 316–375.

Table 1

forcing	period	ΔAMOC [Sv/century]	ΔSTI [K/century]	α_{STI} [Sv/K]	r^2_{STI}	α_{NHT} [Sv/K]	r^2_{NHT}
all-forcing (large) ensemble	1921-2080	-7.0 ± 0.4	-2.3 ± 0.1	3.0 ± 0.1	0.91 ± 0.01	-2.5 ± 0.1	0.93 ± 0.01
	1921-2000	-0.7 ± 1.5	-0.7 ± 0.2	4.0 ± 1.7	0.05 ± 0.09	6.6 ± 5.9	0.02 ± 0.04
	2001-2080	-12.6 ± 1.2	-4.2 ± 0.3	2.8 ± 0.2	0.89 ± 0.02	-2.3 ± 0.2	0.94 ± 0.02
LE #1	1850-2100	-0.5	-0.2	3.1	0.91	-2.6	0.92

Externally-Forced (ensemble mean)

forcing	period	ΔAMOC [Sv/century]	ΔSTI [K/century]	α_{STI} [Sv/K]	r^2_{STI}	α_{NHT} [Sv/K]	r^2_{NHT}
all-forcing	1921-2000	-0.9	-0.7	3.6	0.29	-5.0	0.01
	2001-2080	-12.3	-4.3	2.8	0.98	-2.3	0.98
GHG	1921-2000	-3.2	-1.2	2.8	0.74	-2.8	0.78
	2001-2080	-5.1	-2.7	1.9	0.86	-1.2	0.88
AER	1921-2000	4.5	1.2	3.7	0.86	-4.6	0.85
	2001-2080	-4.5	-1.2	3.8	0.82	-6.1	0.80

Figure 1.

a)

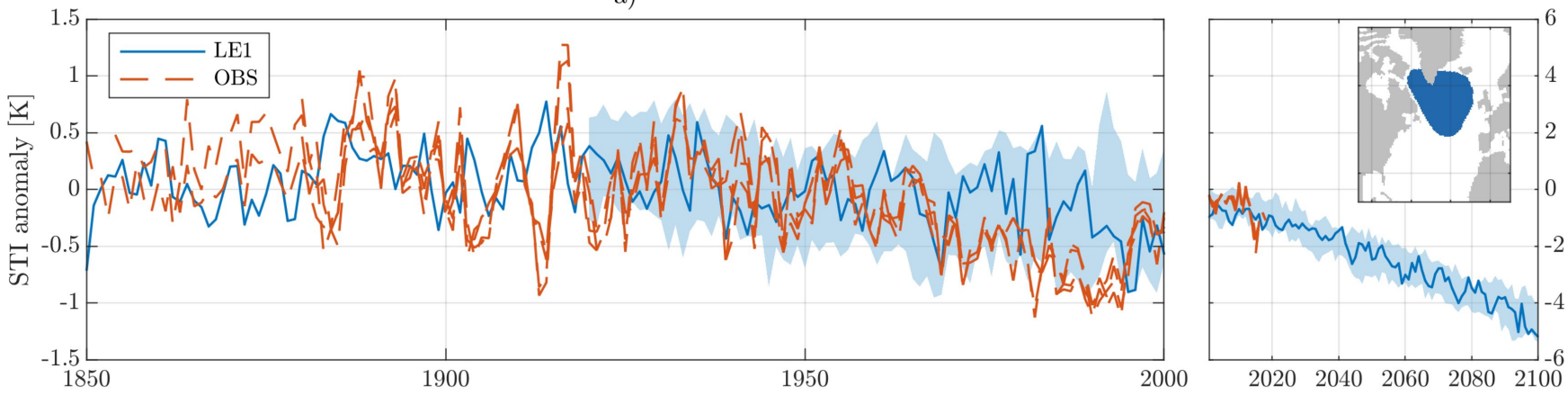
LE1
OBS
STI anomaly [K]
1.5
1
0.5
0
-0.5
-1
-1.5
1850
1900
1950
2000
2020
2040
2060
2080
2100
6
4
2
0
-2
-4
-6

b)

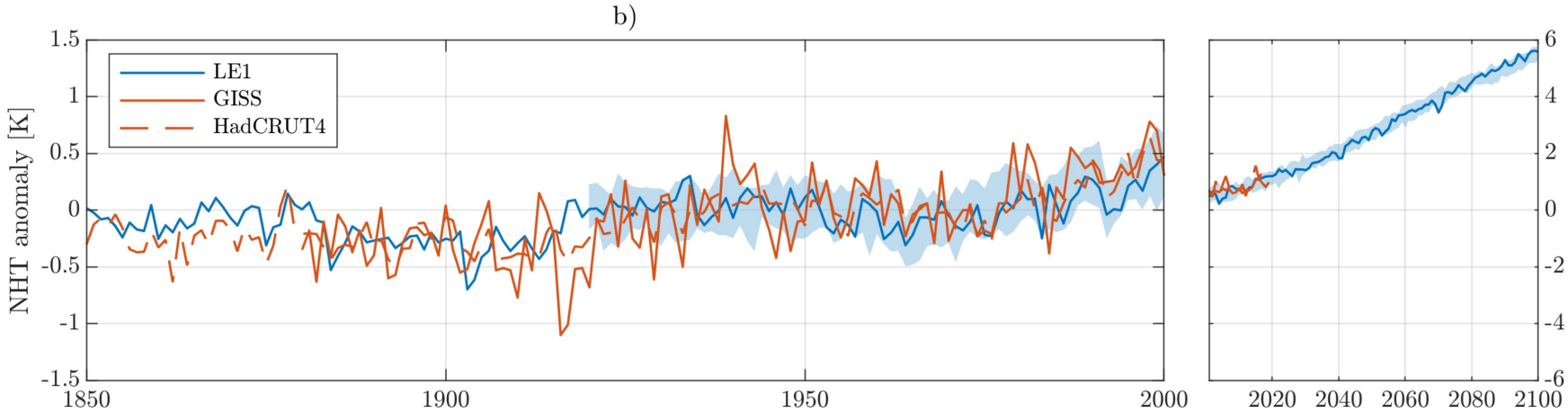
LE1
GISS
HadCRUT4
NHT anomaly [K]
1.5
1
0.5
0
-0.5
-1
-1.5
1850
1900
1950
2000
2020
2040
2060
2080
2100
6
4
2
0
-2
-4
-6

c)

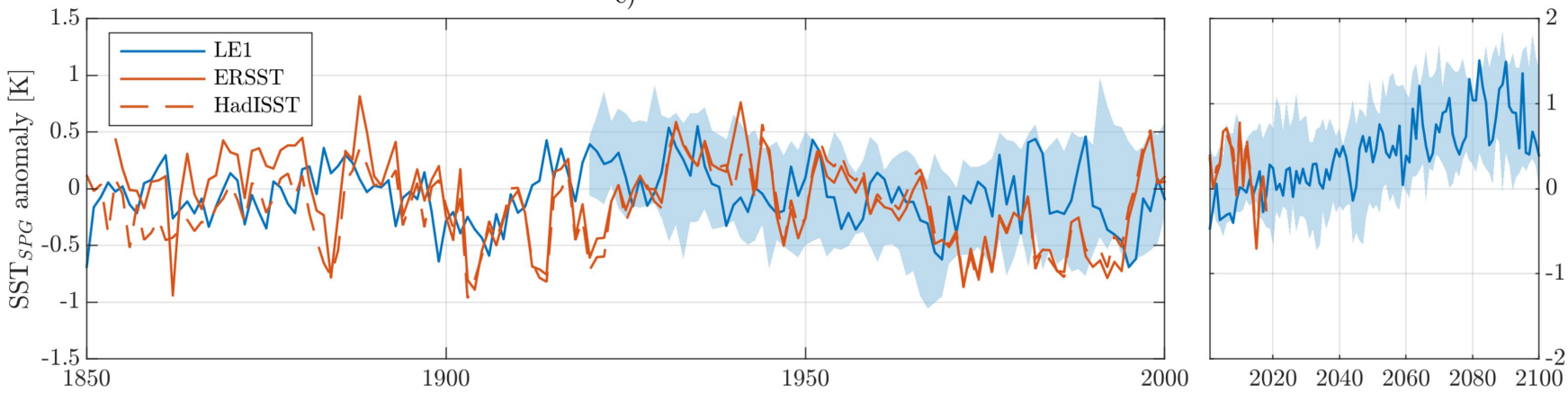
LE1
ERSST
HadISST
SST$_{SPG}$ anomaly [K]
1.5
1
0.5
0
-0.5
-1
-1.5
1850
1900
1950
2000
2020
2040
2060
2080
2100
2
1
0
-1
-2

d)

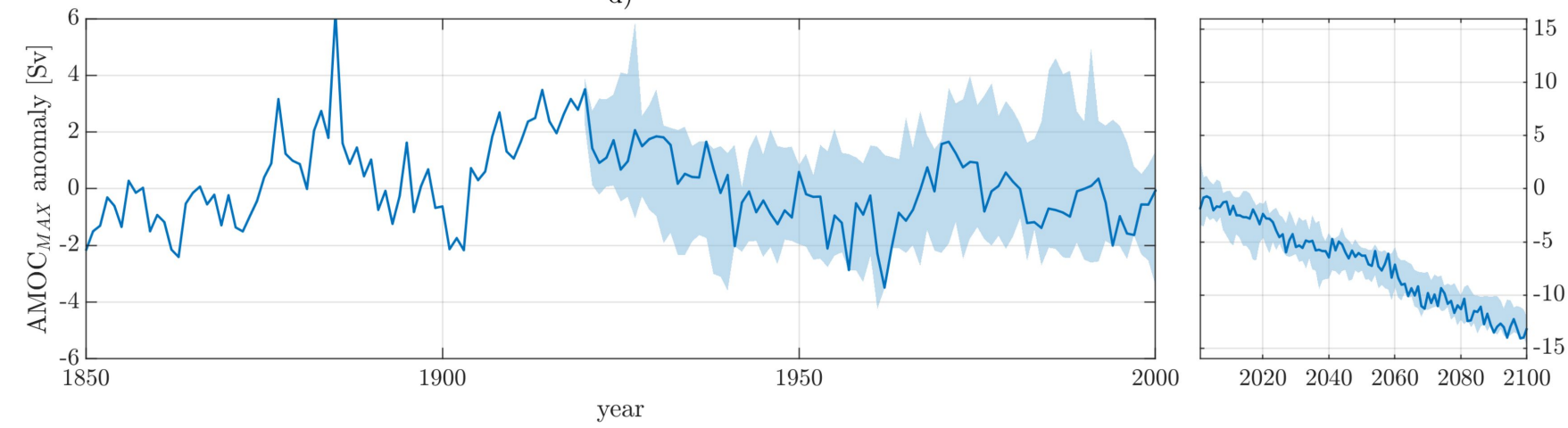
AMOC$_{MAX}$ anomaly [Sv]
6
4
2
0
-2
-4
-6
1850
1900
1950
2000
2020
2040
2060
2080
2100
15
10
5
0
-5
-10
-15
year

Figure 2.

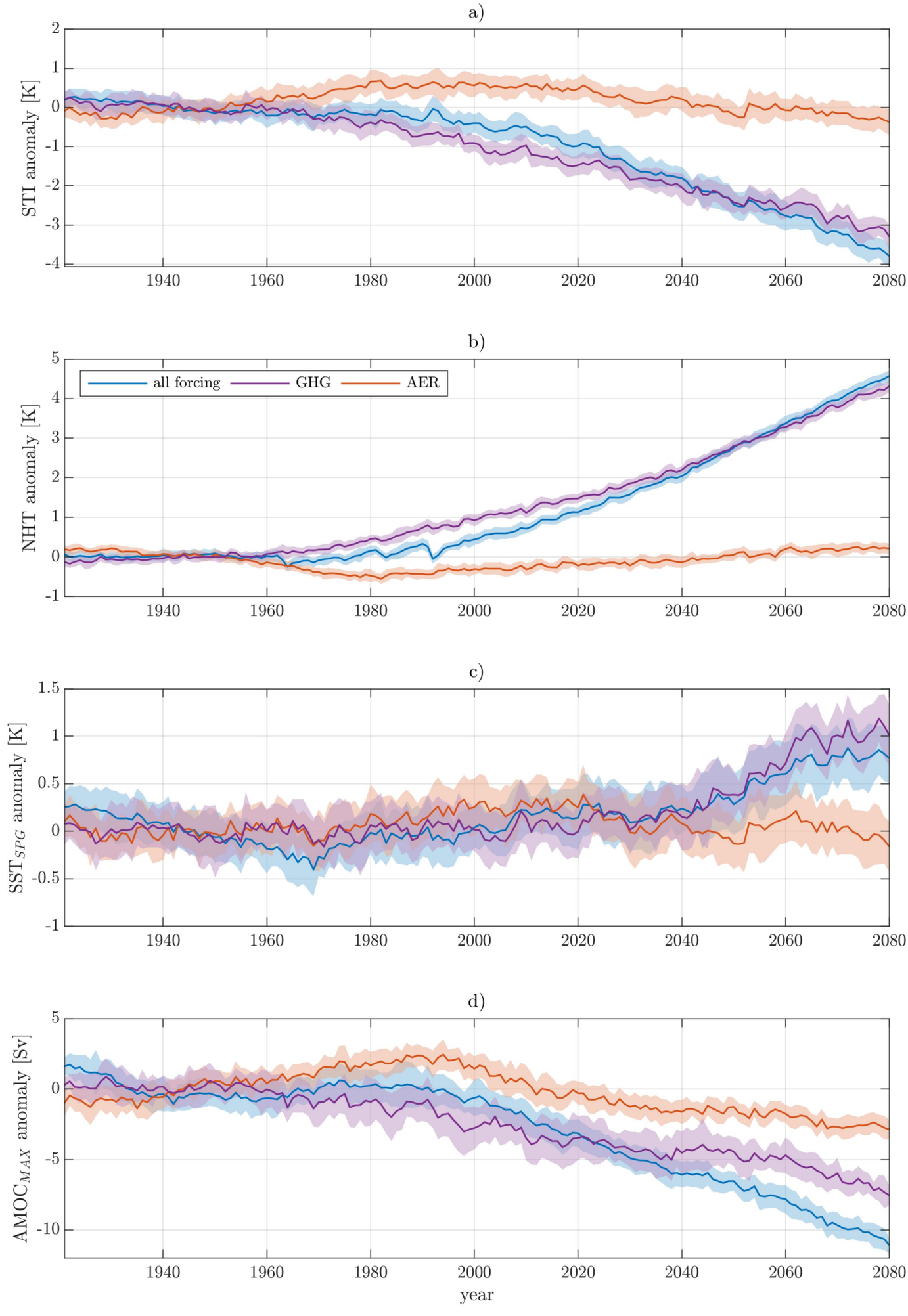
a)
STI anomaly [K]
2
1
0
-1
-2
-3
-4
1940
1960
1980
2000
2020
2040
2060
2080
b)
NHT anomaly [K]
all forcing
GHG
AER
5
4
3
2
1
0
-1
c)
SST$_{SPG}$ anomaly [K]
1.5
1
0.5
0
-0.5
-1
d)
AMOC$_{MAX}$ anomaly [Sv]
5
0
-5
-10
year

Figure 3.

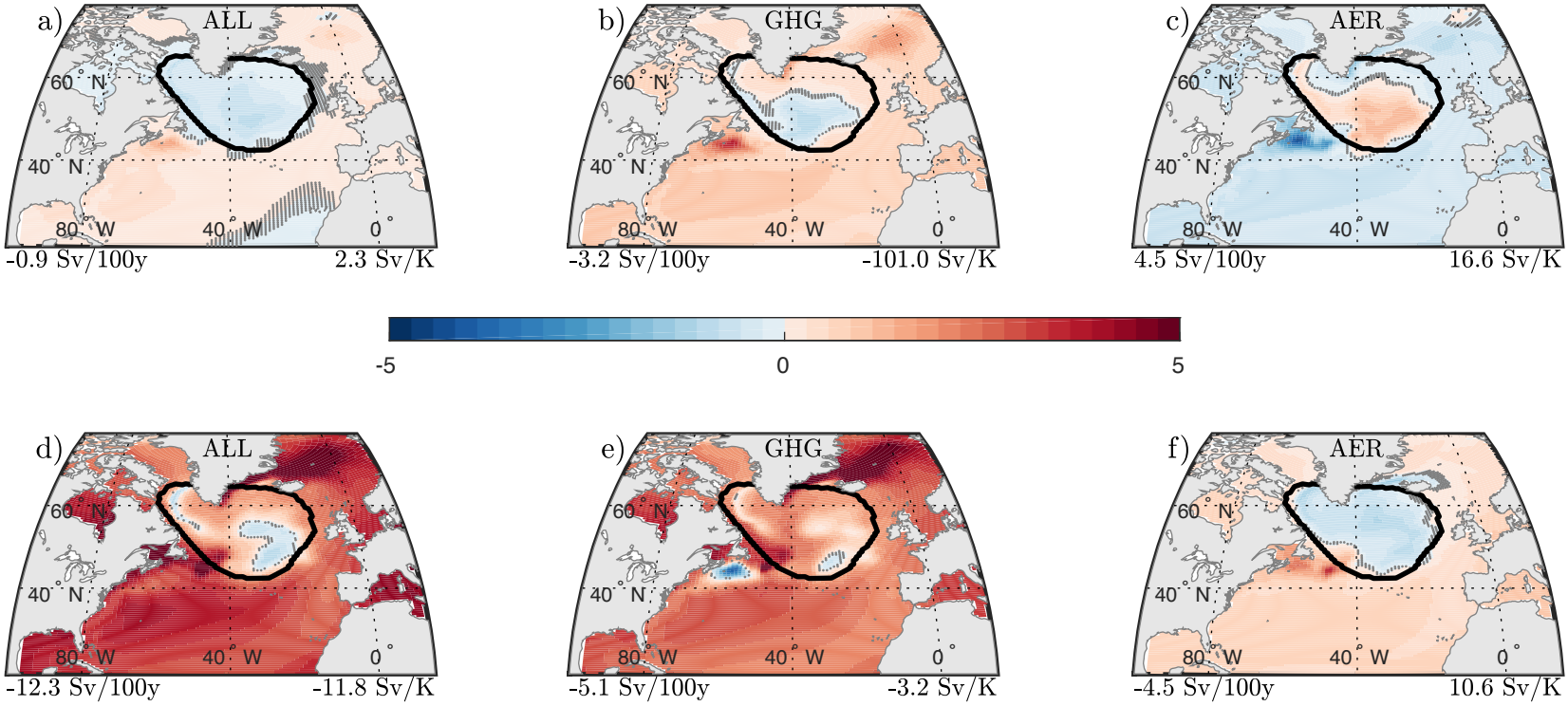
a)
ALL
60° N
40° N
80° W
40° W
0°
-0.9 Sv/100y
2.3 Sv/K
b)
GHG
60° N
40° N
80° W
40° W
0°
-3.2 Sv/100y
-101.0 Sv/K
c)
AER
60° N
40° N
80° W
40° W
0°
4.5 Sv/100y
16.6 Sv/K
-5
0
5
d)
ALL
60° N
40° N
80° W
40° W
0°
-12.3 Sv/100y
-11.8 Sv/K
e)
GHG
60° N
40° N
80° W
40° W
0°
-5.1 Sv/100y
-3.2 Sv/K
f)
AER
60° N
40° N
80° W
40° W
0°
-4.5 Sv/100y
10.6 Sv/K

Figure 4.

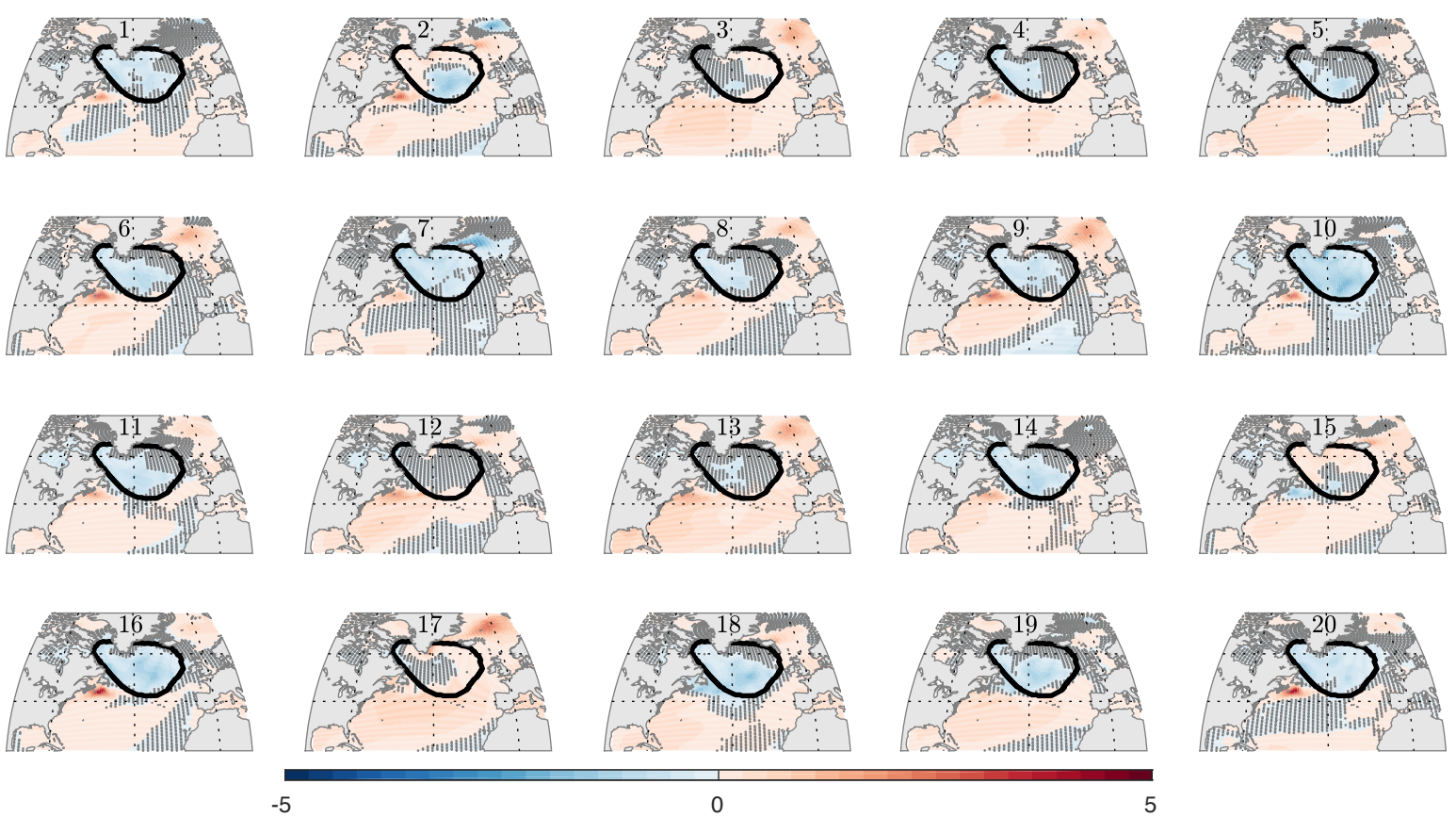
1
2
3
4
5
6
7
8
9
10
11
12
13
14
15
16
17
18
19
20
-5
0
5